Congresso de Métodos Numéricos em Engenharia 2015
Lisboa, 29 de Junho a 2 de Julho, 2015

INFLUENCE OF THE OPTICAL TISSUE PARAMETERS ON THE TRANSMITTED AND REFLECTED SIGNALS FROM A SHORT-PULSE LASER

Pedro Pereira[1], Pedro J. Coelho[1] and Maxime Roger[2]

1: LAETA, IDMEC, Instituto Superior Técnico, Universidade de Lisboa,
Av. Rovisco Pais 1, 1049-001 Lisboa, Portugal
e-mail: pmcpereira7@gmail.com, pedro.coelho@tecnico.ulisboa.pt

2: Université de Lyon, INSA de Lyon, CETHIL, UMR5008, F-69621 Villeurbanne Cedex, France
e-mail: maxime.roger@insa-lyon.fr

Keywords: Thermal radiation, Discrete ordinates method, Discretization schemes, Optical parameters, Short-pulse laser

Abstract *Short-pulse lasers have been used for diagnostic purposes and treatment of tumours in biological tissues in the last few decades. The transmitted and reflected signals are strongly influenced by the optical properties of the tissue, namely the optical thickness of the medium, the scattering albedo, and the scattering phase-function. The purpose of this work is to investigate this dependence by means of the numerical solution of the transient radiative transfer equation. This equation is solved using the discrete ordinates method, and the numerical solution is compared with benchmark results evaluated using the Monte Carlo method. The spatial, temporal and angular discretizations are carried out using the finite volume method along with the second-order accurate CLAM scheme, the second-order Runge-Kutta scheme and the S_N quadrature, respectively. The Henyey-Greenstein scattering phase-function, characterized by its asymmetry factor, is considered. When the asymmetry factor is high, a fine grid is required and the scattering phase function needs to be normalized to obtain an accurate solution. The calculations are performed for a cubical domain with a short-pulse laser incident on one of the faces. The collimated incident radiation is uniform in space and Gaussian in time. The results show that the intensity of the transmitted signal decreases with the increase of the optical thickness, and increases with the increase of the albedo and/or asymmetry factor. The reflected signal is approximately independent of the optical thickness of the medium, increases with the increase of the albedo, and decreases with the increase of the asymmetry factor.*

1. INTRODUCTION

Short-pulse lasers provide many possibilities for applications in materials processing [1], rapid prototyping [2], optical communication [3], optical measurements [4], biomedical imaging, diagnosis and treatment [5]. Short-pulse lasers have emerged in the last 20-30 years as an effective tool in biomedical diagnosis and treatment. The number of people suffering from tumours all over the world is very large, and this number is unlikely to decrease in the middle term. Therefore, the diagnosis of tumours is of major relevance, and short-pulse lasers may be used for that purpose. Although continuous-wave lasers are often used in medicine, short-pulse lasers have the advantage of delivering the required amount of energy to the desired zone to be probed or treated (e.g., a tumour) in a short time period, and therefore are less aggressive.

In the case of ultrafast pulse lasers, with a duration ranging from picoseconds to femtoseconds, the thermal relaxation time of the biological tissue is several orders of magnitude greater than the pulse-width, so that the heat affected zone affected is limited to the laser region, and the increase of temperature of the neighbouring tissue is negligible. Moreover, the rise of temperature in the medium is too small to affect light propagation, and in particular the back-scattered and transmitted laser signatures, which are useful for diagnosis purposes. Therefore, most studies that investigate the light propagation in tissues consider the medium as cold, and are just concerned with the temporal signature of the laser.

The scattered temporal signature persists for a long time, compared with the pulse width, and depends on the optical properties of the medium. Tumours have optical properties different from those of healthy tissues, and the back-scattered/transmitted signals are different depending on the size and location of the tumour [6-7]. However, because of the highly anisotropic scattering nature of biological tissues, direct reconstruction methods cannot be used, and an inverse-based reconstruction technique is needed to estimate the optical properties of the medium based on the back-scattered and/or transmitted light. This method, referred to as diffuse optical tomography, is a typical example of a non-invasive diagnosis method that uses short pulse lasers [8-9].

In this context, this work is concerned with the investigation of the reflected and transmitted signals from a short-pulse laser in a medium with optical properties typical of biological tissue, and on the influence of these properties on those signals. We are not concerned with a real application in the present paper, but the short/medium term objective is to investigate the use of short-pulse lasers for diagnosis and laser-induced hyperthermia therapy of skin tissue.

The propagation of light from a laser in a tissue is described by the transient radiative transfer equation. Many numerical methods have been developed to solve this equation, such as the P1 approximation, the discrete ordinates method (DOM), the finite volume method and the Monte Carlo (MC) method, among others [10]. Here, we will use both the DOM and the MC method. The later is mostly used to obtain reference solutions, while the former provides a

better compromise between accuracy and computational requirements. The DOM is briefly explained in the next section, which is followed by the description of the test case. The results obtained are then presented and discussed, and the paper ends with a summary of the main conclusions.

2. THEORY

A brief overview of the discretization of the radiative transfer equation (RTE) using the DOM is presented below. The RTE for an emitting-absorbing-scattering grey medium may be written as follows [11]:

$$\frac{1}{c}\frac{\partial I(\mathbf{r},\mathbf{s},t)}{\partial t}+\mathbf{s}\cdot\nabla I(\mathbf{r},\mathbf{s},t)=-\beta I(\mathbf{r},\mathbf{s},t)+\kappa I_b(\mathbf{r})+\frac{\sigma_s}{4\pi}\int_{4\pi} I(\mathbf{r},\mathbf{s}',t)\,\Phi(\mathbf{s}',\mathbf{s})\,d\Omega' \qquad (1)$$

where $I(\mathbf{r},\mathbf{s},t)$ is the radiation intensity at position **r,** in direction **s**, and at time t, I_b the blackbody radiation intensity, c the speed of light, κ; β and σ_s the absorption, extinction and scattering coefficients of the medium, respectively, $\Phi(\mathbf{s}',\mathbf{s})$ the scattering phase function and Ω a solid angle.

The spatial discretization in the DOM is obtained using the finite volume method. Hence, integrating the RTE in time over a control volume centred at grid node P, and applying the Gauss divergence theorem to the second term on the left hand side, yields

$$\begin{aligned}&\frac{1}{c}\frac{\partial I_P(\mathbf{s},t)}{\partial t}V+\int_A \mathbf{s}\cdot\mathbf{n}\,I(\mathbf{r},\mathbf{s},t)\,dA=\\&\quad=-\beta V I_P(\mathbf{s},t)+\kappa V I_{b,P}+\frac{\sigma_s}{4\pi}V\int_{4\pi} I_P(\mathbf{s}',t)\,\Phi(\mathbf{s}',\mathbf{s})\,d\Omega'\end{aligned} \qquad (2)$$

where **n** denotes the outer unit vector normal to a cell face, and V is the volume of the control volume under consideration. Equation (2) was obtained assuming that the radiation intensity and the radiative properties remain constant within the control volume, following the standard finite volume discretization procedure. The integral along the boundary on the left side of equation (2) is now approximated by a summation, yielding

$$\begin{aligned}&\frac{1}{c}\frac{\partial I_P(\mathbf{s},t)}{\partial t}V+\sum_{f=1}^{F}\mathbf{s}\cdot\mathbf{n}_f\,I_f(\mathbf{s},t)\,A_f=\\&\quad=-\beta V I_P(\mathbf{s},t)+\kappa V I_{b,P}+\frac{\sigma_s}{4\pi}V\int_{4\pi} I_P(\mathbf{s}',t)\,\Phi(\mathbf{s}',\mathbf{s})\,d\Omega'\end{aligned} \qquad (3)$$

where subscript *f* denotes a cell face, whose area is A_f, F is the total number of cell faces of the control volume under consideration, and $I_f(\mathbf{s})$ the mean radiation intensity at cell face *f* along direction **s.**

Different methods may be employed to relate $I_f(\mathbf{s})$ to the radiation intensity at the grid nodes. In this work we used the second-order CLAM scheme [12] which approximates $I_f(\mathbf{s})$ as a function of the radiation intensity at the grid node immediately downstream of the cell face, denoted by subscript *D*, and at the two grid nodes upstream of the cell face, denoted by subscripts *C*, for the grid node closest to the cell face, and *U*, for its upstream neighbour. As an example, if radiation is propagating in positive *x* direction, the calculation of the radiation intensity at cell face i+1/2 of the control volume centred at grid node i is obtained from the radiation intensities at grid nodes i+1 (*D*), i (*C*) and i-1 (*U*). If radiation propagates along the negative *x* direction, the radiation intensity at the same cell face, i+1/2, is expressed in terms of the radiation intensities at grid nodes i (*D*), i+1 (*C*) and i+2 (*U*). The following expressions are used to determine the cell face radiation intensities:

$$I_f = \begin{cases} I_U + (I_C - I_U)\left(2 - \dfrac{I_C - I_U}{I_D - I_U}\right) & \text{if} \quad 0 \le \dfrac{I_C - I_U}{I_D - I_U} \le 1 \\ I_C \quad \text{if} \quad \dfrac{I_C - I_U}{I_D - I_U} \le 0 \quad \text{or} \quad \dfrac{I_C - I_U}{I_D - I_U} \ge 1 \end{cases} \tag{4}$$

The time discretization was carried out using the second-order explicit Runge-Kutta scheme. Let us express equation (3) in the form

$$\frac{1}{c}\frac{\partial I_P}{\partial t} V = f(I_P, t) \tag{5}$$

where

$$f(I_P, t) = -\sum_{f=1}^{F} \mathbf{s}\cdot\mathbf{n}_f \; I_f(\mathbf{s},t)\, A_f - \beta V I_P(\mathbf{s},t) + \kappa V \; I_{b,P} + \frac{\sigma_s}{4\pi} V \int_{4\pi} I_P(\mathbf{s}',t)\, \Phi(\mathbf{s}',\mathbf{s})\, d\Omega' \tag{6}$$

The time discretization then yields

$$\frac{I_P^{n+1} - I_P^n}{c\,\Delta t} V = f\left(I_P^n + \frac{\Delta t}{2} f\left(I_P^n, t^n\right), t^n + \frac{\Delta t}{2}\right) \tag{7}$$

Superscripts n and n+1 denote the lower and upper limits of the time step Δt.

The angular discretization in the DOM is carried out by replacing the RTE by a discrete set of M coupled differential equations that describe the radiation intensity field along M directions. Integrals over solid angles are replaced by a quadrature of order M yielding the following discretized equation for the DOM:

$$\frac{I_P^{m,n+1} - I_P^{m,n}}{c\,\Delta t} V = f\left(I_P^{m,n} + \frac{\Delta t}{2} f\left(I_P^{m,n}, t^n\right), t^n + \frac{\Delta t}{2} \right) \tag{8}$$

with

$$f\left(I_P^{m,n}, t^n\right) = -\sum_{f=1}^{F} \mathbf{s}^m \cdot \mathbf{n}_f \; I_f^{m,n} \; A_f - \beta V I_P^{m,n} + \kappa V \; I_{b,P} + \frac{\sigma_s}{4\pi} V \sum_{l=1}^{M} w_l \; I_P^{l,n} \; \Phi\left(\mathbf{s}^l, \mathbf{s}^m\right) \tag{9}$$

where superscript m ($1 \leq m \leq M$) denotes the mth direction and w_l is the quadrature weight for the lth direction.

When the medium is subjected to laser irradiance, as in the present work, it is convenient to decompose the radiation intensity into its collimated component, I_c, and its diffuse component, I_d, according to $I(\mathbf{r},\mathbf{s},t) = I_c(\mathbf{r},t) + I_d(\mathbf{r},\mathbf{s},t)$. In this case, the RTE is expressed by the two following equations:

$$\frac{1}{c}\frac{\partial I_c}{\partial t} + \mathbf{s} \cdot \nabla I_c = -\beta I_c \tag{10}$$

$$\frac{1}{c}\frac{\partial I_d}{\partial t} + \mathbf{s} \cdot \nabla I_d = -\beta I_d + \kappa I_b + \frac{\sigma_s}{4\pi} \int_{4\pi} \Phi\left(\mathbf{s} \cdot \mathbf{s}'\right) I_d' \, d\mathbf{s}' + \frac{\sigma_s}{4\pi} \Phi\left(\mathbf{s} \cdot \mathbf{s}_c\right) I_c \tag{11}$$

Subscripts c and d stand for the collimated and diffusive components, respectively. The collimated component is only different from zero along the direction defined by the unit vector $\mathbf{s}_c$. Equation (10) may be solved analytically, and the following solution is obtained:

$$I_c(\mathbf{r},t) = I_c\left(\mathbf{r}_w, t_w\right) \exp\left(- \int_0^{\|\mathbf{r} - \mathbf{r}_w\|} \beta \, ds \right) \tag{12}$$

where $t_w = t - \|\mathbf{r} - \mathbf{r}_w\| / c$ and $\mathbf{r}_w$ is the position vector of a boundary point, where the

collimated radiation component is prescribed. This result is inserted in equation (11), which is discretized as described above.

3. TEST CASE

The problem addressed in this work consists of a cubic domain of side L=1 m, schematically shown in Figure 1, containing a scattering and absorbing homogeneous medium and subjected to an incident laser source propagating along x direction, while the remaining boundaries are non-reflecting and cold (non-emitting). The medium is cold, as often considered in problems of light propagation in biological tissues, and the scattering is described by the Henyey-Greenstein phase function [11]. The intensity of the short-pulse laser, Gaussian in time and uniform in space, is given by

$$I_c(x=0,t) = I_o \; exp\left[-4(ln\,2)\left(\left(t-3t_p\right)/t_p\right)^2\right] , \quad 0<t<6t_p \tag{13}$$

where x = 0 is the emitting wall location, and I_o is the maximum radiative intensity of the pulse, which occurs at $t = 3t_p = 1.5/\beta c$. After $6t_p$, the medium is free from irradiation. In this work we are concerned with the temporal signature of the radiation leaving from the boundary opposite to the laser source, $x = L$, and with the reflected signal at $x = 0$. These are quantified by the dimensionless transmittance and reflectance signals given by

$$T(t) = \frac{1}{I_o\, L^2}\int_0^L\int_0^L \left(I_c(x=L,y,z,t) + \int_{2\pi} I_d(x=L,y,z,\mathbf{s},t)(\mathbf{s}\cdot\mathbf{i})d\mathbf{s} \right) dy\,dz \tag{14}$$

$$R(t) = \frac{1}{I_o\, L^2}\int_0^L\int_0^L\int_{2\pi} I_d(x=0,y,z,\mathbf{s},t)(-\mathbf{s}\cdot\mathbf{i})d\mathbf{s}\,dy\,dz \tag{15}$$

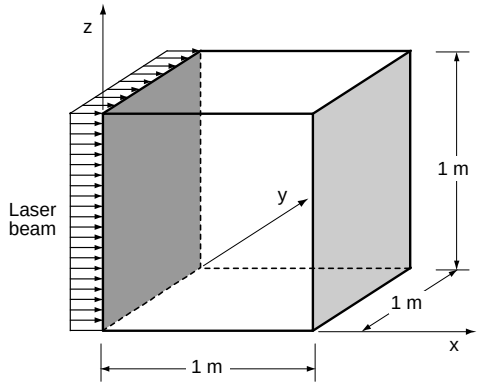

Figure 1. Schematic of the test case.

where **i** is the unit vector in positive x direction. A previously validated Monte Carlo algorithm [13] was used to provide benchmark results. The spatial domain was discretized using a uniform grid with 50×20×20 control volumes and an S_{12} quadrature was employed for most calculations. Exceptions will be identified in the next section. The time step Δt for the DOM was defined as $\Delta t=\alpha.\Delta x/c$, where the stability parameter α was set equal to 0.5.

4. RESULTS AND DISCUSSION

We first consider a medium with an optical thickness $\tau = \beta L = 10$ and an albedo $\omega = \sigma_s / \beta = 0.5$. The predicted transmittance and reflectance signals for the DOM and MC method are displayed in Figure 2. The predictions are shown for an isotropically scattering medium (g=0) and for a moderately forward scattering medium (g=0.3), where g stands for the asymmetry factor of the scattering phase function.

The DOM predictions are in relatively good agreement with the MC reference solution, despite a slight overprediction of the peak value of the transmittance and reflectance. The transmittance is initially equal to zero, since photons must travel throughout the medium before they reach the boundary $x = L$. The photons travel at the speed of light, and therefore those that are not scattered in the medium need a time equal to L/c = 3.33 nanoseconds to

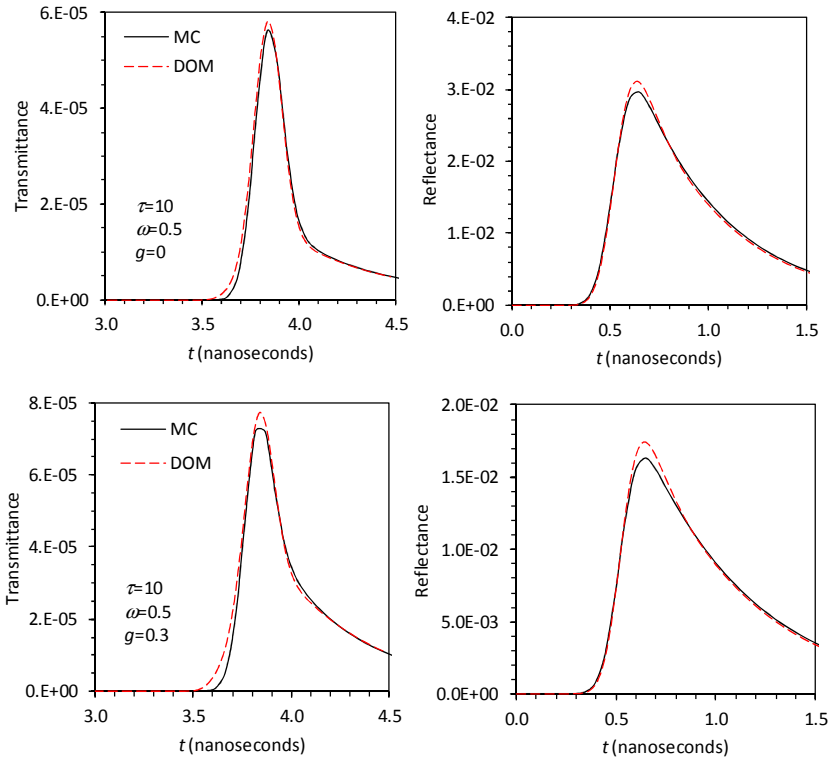

Figure 2. Predicted transmittance and reflectance for $\tau = 10$ and $\omega = 0.5$.

reach that boundary, and consequently the transmittance signal is different from zero only after that time. However, the transmittance becomes only significant a little later, due to the Gaussian nature of the incident pulse. The transmittance exhibits a sharp peak and a Gaussian like shape, due to the collimated radiation component that is able to travel across the medium without being fully absorbed. Downstream of the peak of the transmittance, the signal exhibits a strong decrease, but it does not drop to zero. Instead, the transmittance remains positive for some more time, due to the contribution of the diffuse component arising from scattering within the medium, i.e., from photons scattered within the medium, which take more time to reach the boundary. When forward scattering is considered, the peak of the transmittance increases, and so does the transmittance thereafter, due to the greater number of photons that are scattered forward.

The reflectance signal is entirely due to photons that are scattered backward. Therefore, the reflectance decreases with the increase of the asymmetry factor. The intensity of the short-pulse laser only becomes significant after 0.3 nanoseconds, and achieves its maximum value at 0.5 nanoseconds for τ = 10. Therefore, the reflectance increases rapidly after 0.3 nanoseconds, and achieves a maximum shortly after the peak of the Gaussian pulse occurs. Then, it decreases slowly, as the number of back scattered photons that reach the x = 0 boundary decreases.

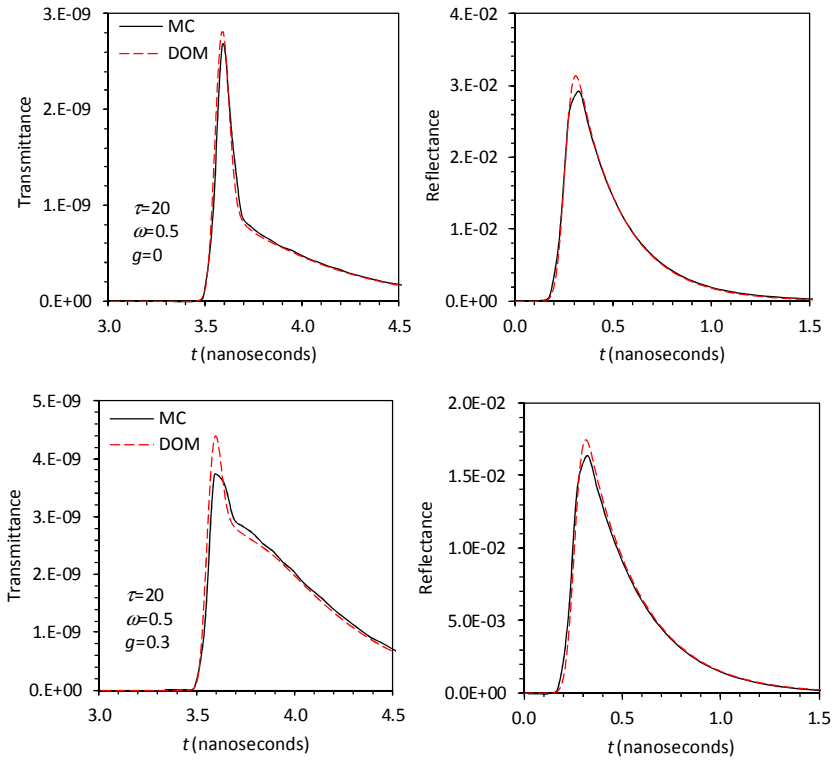

Figure 3. Predicted transmittance and reflectance for τ = 20 and ω = 0.5.

Figure 3 shows the transmittance and reflectance for a medium with $\tau = 20$ and $\omega = 0.5$. In this case, the width of the Gaussian laser pulse is smaller, and therefore a finer grid in streamwise direction was used, the number of grid nodes being 200×20×20. This was needed to predict satisfactorily the sharp rise of the transmittance signal when using the DOM. Otherwise, the predictions are not satisfactory, particularly for $g = 0.3$. Despite this, the peak of the transmittance was overestimated by about 15%.

The transmittance signal is about four orders of magnitude smaller than in the previous case, beacuse of the stronger optical thickness of the medium, and it occurs earlier since the reduction of the pulse width implies that the peak of the laser pulse is also attained earlier. Accordingly, the first photons also reach the boundary $x = L$ earlier than for $\tau = 10$, and a sharper increase of the transmittance is then observed. The asymmetry of the transmittance signal is due to the role of the forward scattered photons, which imply that the transmittance decrases slowly a little after the maximum has been observed. In fact, the marked change in the slope of the transmittance signal at $\tau \approx 3.7$ nanoseconds is due to the dominant role of the collimated radiation component before that time, in contrast to the dominant role of the diffuse component thereafter. The reflectance exhibits a peak that is approximately independent of the optical thickness of the medium, but which occurs earlier when the optical thickness increases, due to the reasons discussed above, i.e., because of the shorter incident pulse width.

Figure 4 shows the results obatined for $\tau = 20$ and $\omega = 0.9$. Four different values of the asymmetry factor have been considered, ranging from an isotropic medium ($g = 0$) up to a strongly forward scattering medium ($g = 0.9$). In the last case, a mesh with 200×50×50 grid nodes was used, and the scattering phase function was normalized according to the method proposed by Hunter and Guo [14] for the DOM. This was needed to obtain satisfactory results, as discussed elsewhere [15, 16]. The MC predictions exhibit small oscillations, which are due to the statistical nature of the method. These could be eliminated at the expense of additional computing time, but this was not deemed necessary for the purpose of the present work. In general, the DOM predictions are in good agreement with the MC solution. Only in the most challenging case, corresponding to $g = 0.9$, the discrepancies are a little higher, with the peak of the transmittance being underestimated by about 15%.

In the present case ($\tau = 20$, $\omega = 0.9$), the contribution of the diffuse radiation component to the transmittance is dominant, while the collimated component has a negligible contribution. In fact, the transmittance for $\tau = 20$ and $\omega = 0.5$ was of the order of 10^{-9}, while in the present case, with a much higher scattering coefficient, the order of magnitude increases with the asymmetry factor from 10^{-7}, in the case of isotropic scattering, up to 10^{-3} in the case of $g = 0.9$. In contrast to previous cases, there is no sharp peak of the transmittance for the present optical parameters, due to the dominance of the diffuse radiation component. The maximum transmittance occurs progressively earlier, and becomes more pronounced, as the asymmetry factor increases. The reflectance displays a peak that occurs at the same time observed for $\tau =$

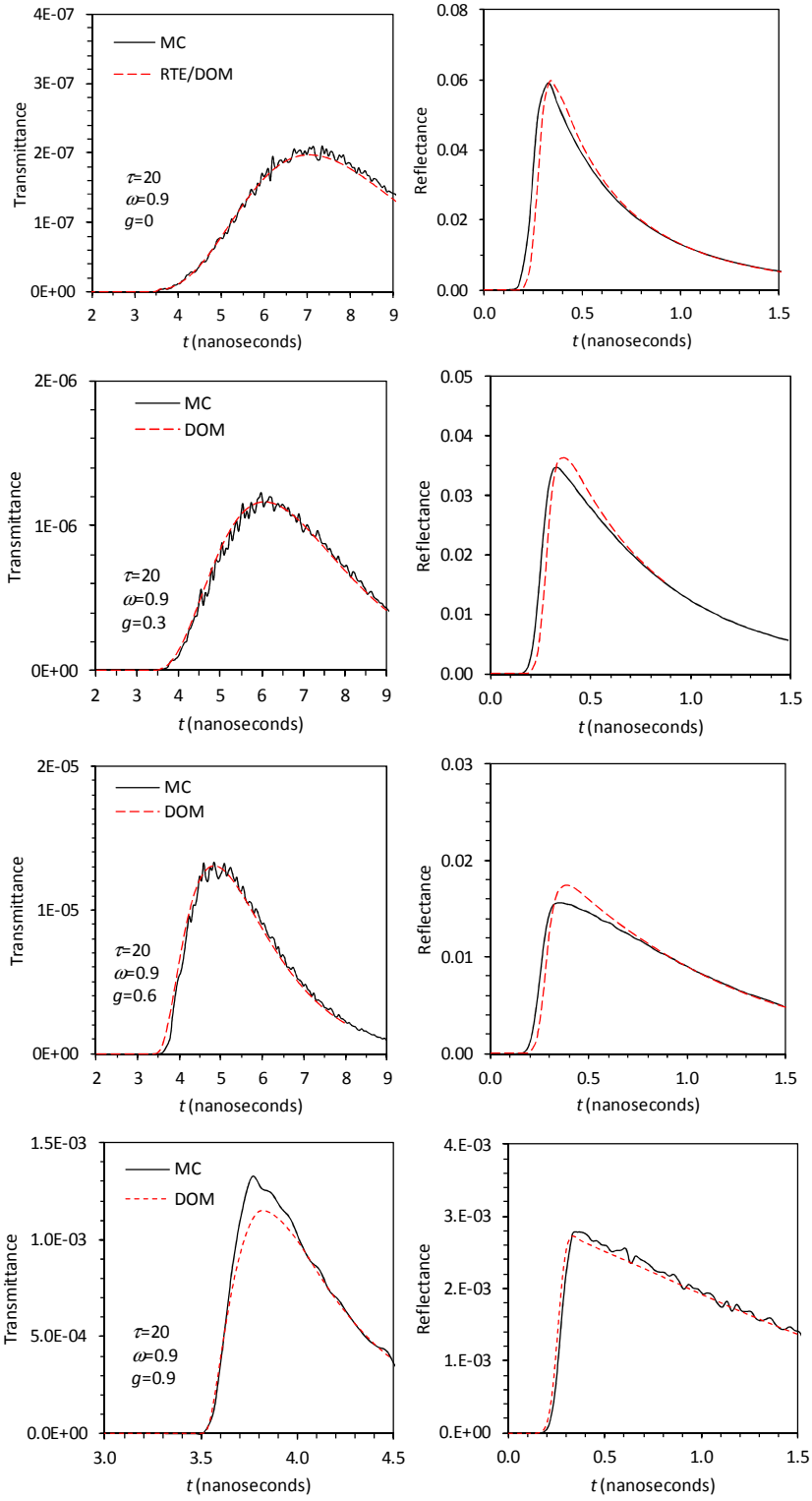

Figure 4. Predicted transmittance and reflectance for $\tau = 20$ and $\omega = 0.9$.

20 and $\omega = 0.5$, i.e., the time at which it appears is independent of the albedo and asymmetry factor, depending only on the optical thickness of the medium. As the asymmetry factor increases, the reflectance signal becomes weaker, and decays slower after the maximum is attained.

Further insight into the influence of the optical parameters of the medium on the transmittance signal is provided by Figure 5, which illustrates the influence of the optical thickness, the albedo and the asymmetry factor of the scattering phase function on the peak of the transmittance, and on the time at which it occurs. In the case of an optical thickness of unity, the maximum transmittance is approximately independent of the albedo and asymmetry factor (see Figures 5a and 5c), because the collimated component is dominant in this case, while the diffuse component plays a negligible role. When $\tau = 10$, the maximum transmittance increases slightly as the anisotropy of the phase function becomes stronger, as formerly observed in Figure 2, while a greater influence is observed for $\tau = 20$ (see Figure 5a, as well as Figures 3 and 4). The time at which the maximum transmittance occurs is higher for $\tau = 1$ than for optically thick media, and it is approximately independent of the asymmetry factor for $\omega = 0.5$, while it decreases with the increase of the asymmetry factor for $\omega = 0.9$ (see Figure 5b), as discussed above (see Figures 3 and 4).

Figure 5(c) further reveals a consistent decrease of the maximum transmittance with the increase of the optical thickness of the medium, provided that the albedo and the asymmetry factor remain constant. Figure 5(d) shows that the time at which the maximum occurs is greater for $\tau = 1$ than for optically thick media. In the case $\tau = 1$, neither the albedo nor the scattering phase function influence that time, because the collimated radiation component prevails. In the case of optically thick media, the maximum transmittance appears at a time that marginally decreases with the increase of the optical thickness and is independent of the asymmetry factor for $\omega = 0.5$, since the collimated component still dominates. However, for $\omega = 0.9$, the diffuse component dominates, as observed in Figure 4, and therefore the time corresponding to the peak transmittance is larger, and increases with the increase of the optical thickness.

The influence of the albedo is illustrated in Figures 5(e) and 5(f). When $\tau = 10$ and $g = 0$, the albedo does not influence the maximum of the transmittance, but this maximum appears later when the albedo increases. When $\tau = 20$, the transmittance peak increases and its occurrence is delayed with the increase of the albedo, since the collimated component becomes lower than the diffuse component when ω is close to unity, as previously shown in Figure 4.

5. CONCLUSIONS

The DOM was used to investigate the influence of the optical thickness of the medium, scattering albedo and asymmetry factor of the scattering phase function on the transmittance and reflectance signals from a short-pulse laser. The results were validated by means of

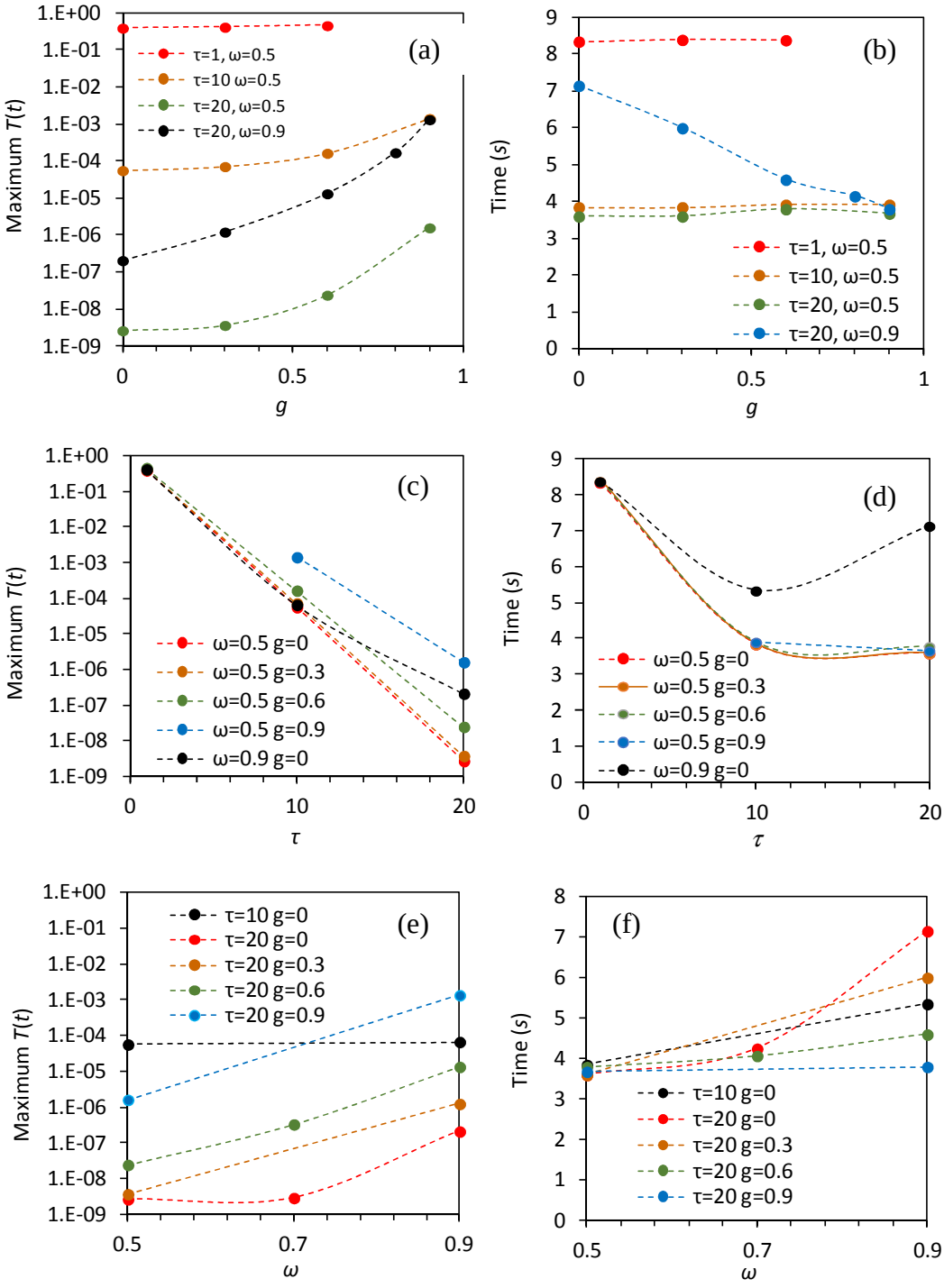

Figure 5. Influence of the optical parameters on the peak of the transmittance and on the time at which it occurs.

comparison with Monte Carlo reference solutions. The following main conclusion may be drawn from the analysis carried out:

1. In the case of a low or moderate optical thickness, the transmittance exhibits a sharp peak, due to the dominating contribution of the collimated radiation component over the diffuse component. In that case, the time at which the maximum transmittance occurs is only dictated by the optical thickness of the medium. The peak transmittance decreases with the increase of the optical thickness of the medium, and the diffuse component becomes dominant for strongly forward scattering media. In the last case, the peak transmittance occurs earlier for larger asymmetry factor of the phase function.

2. The maximum transmittance increases with the increase of the albedo and/or asymmetry factor, except for small optical thickness, since in the last case the diffuse component does not influence that maximum.

3. The reflectance exhibits a maximum that is independent of the optical thickness of the medium, increases with the increase of the albedo, and decreases with the increase of the asymmetry factor. The maximum reflectance occurs at a time that is only a function of the optical thickness the medium, due to the dependence of the incident pulse width on the optical thickness.

ACKNOWLEDGEMENTS

This work was financially supported by national funds through FCT-Fundação para a Ciência e Tecnologia under the project PTDC/EMS-ENE/1028/2012.

REFERENCES

[1] K. Sugioka and Y. Cheng, “Ultrafast lasers — reliable tools for advanced materials processing”, *Light: Science & Applications*, Vol. **3**, e149 (2014).

[2] P. K. Venuvinod and W. Ma, *Rapid prototyping: laser-based and other technologies*, Kluwer Academic Publishers (2004).

[3] K. R. Tamura, “Short pulse lasers and their applications to optical communications”, LEOS '99. IEEE Lasers and Electro-Optics Society, 12th Annual Meeting, Vol. 2, pp. 537-538 (1999).

[4] J. R. Gord, T. R. Meyer and S. Roy, “Applications of ultrafast lasers for optical measurements in combusting flows”, *Annual Review of Analytical Chemistry*, Vol. **1**, 663-687 (2008)

[5] A. J. Welch and M. J. C. van Gemert (eds.), *Optical-thermal response of laser-irradiated tissue*, 2nd ed., Springer (2011).

[6] M. Sakami and K. Mitra, “Analysis of short-pulse laser photons transport through

tissues for optical tomography", *Optics Letters*, Vol. **17**, pp. 336-338 (2002).
[7] C. Das, A. Trived, K. Mitra and T. Vo-Dinh, "Short pulse laser propagation through tissues for biomedical imaging", *J. Physics D: Applied Physics*, Vol. **36**, pp. 1-8 (2003).
[8] A. Charette, J. Boulanger and H. K. Kim, "An overview of recent radiation transport algorithm development for optical tomography imaging", *J. Quantitative Spectroscopy and Radiative Transfer*, Vol. **109**, pp. 2743-2766 (2008).
[9] O. Balima, Y. Favenned and D. Rousse, "Optical tomography reconstruction algorithm with the finite element method: an optimal approach with regularization tools", *Journal of Computational Physics*, Vol. **251**, pp. 461-479 (2013).
[10] Z. Guo and B. Hunter, "Advances in ultrafast radiative transfer modeling and applications: a review", *Heat Transfer Research*, Vol. **44**, pp. 305-346 (2013).
[11] M. F. Modest, *Radiative heat transfer*, Academic Press, New York (2003).
[12] B. Van Leer, "Towards the ultimate conservation difference scheme. ii. monotonicity and conservation combined in a second-order scheme", *J. Computational Physics*, Vol. 14, pp. 361-370 (1974).
[13] M. Roger, C. Caliot, N. Crouseilles and P. J. Coelho, "A hybrid transport-diffusion model for radiative transfer in absorbing and scattering media". *J. Computational Physics*, Vol. 275, pp. 346-362 (2014).
[14] B. Hunter and Z. Guo, "Conservation of asymmetry factor in phase function discretization for radiative transfer analysis in anisotropic scattering media", *Int. J. Heat Mass Transfer*, Vol. 55, pp 1544–52 (2012).
[15] P. Pereira, M. Roger and P. J. Coelho, "Comparison of different formulations for transient radiative transfer problems in absorbing and scattering three-dimensional media", *5ª Conferência Nacional de Mecânica dos Fluidos, Termodinâmica e Energia*, Porto, Portugal, 11-12 September (2014).
[16] P. Pereira, M. Roger and P. J. Coelho, "Discrete ordinates solution of the radiative transfer equation and multi-scale models for three-dimensional transient problems", *Proceedings of CHT-15 — ICHMT International Symposium on Advances in Computational Heat Transfer*, Rutgers University, Piscataway, New Jersey, 25-29 May (2015).